Visualization of individual DNA molecules in a small-scale coating flow

Rajat Duggal and Matteo Pasquali[a)]

Department of Chemical Engineering, Rice University, MS 362, 6100 Main Street, Houston, Texas 77005

(Received 30 June 2003; final revision received 27 April 2004)

Synopsis

Individual DNA molecules in an ultradilute solution were observed with a fluorescence microscope as they flow between a scaled-down rotating roll and a stationary glass knife. The roll picks up a thin layer of liquid from a pool and drags it to the knife, establishing a bead delineated by two menisci. At low roll speed the flow is premetered and there is a large recirculation. The DNA experiences nearly rectilinear shear flow at the minimum gap position where there is a zero velocity surface. We report the mean and the distribution of fractional extension of DNA molecules and show that the mean fractional extension asymptotes to 0.5, in agreement with the results of Smith *et al.* [D. E. Smith *et al.*, Science **283**, 1724 (1999)]. Interestingly, no polymer distortion is observed at the two menisci. At high roll speed, capillarity is not strong enough to drive backflow; the big recirculation under the coverslip breaks into two smaller recirculations and two separation surfaces arise upstream and downstream of the location of the minimum gap. At the upstream separation surface, most DNA molecules are extended parallel to the knife as they traverse the field of view. We report the distribution of DNA extension and shape in this flow region. Slow, nodular recirculations are present under the upstream and downstream free surfaces. Notably, most DNA molecules stretch axially as they move in these slow recirculating regions. © *2004 The Society of Rheology.* [DOI: 10.1122/1.1764825]

I. INTRODUCTION

Free surface flows of dilute polymer solutions are important in various industrial and biological applications. In these flows, the velocity gradient stretches the polymer molecules, and in turn the stretched polymer molecules change the behavior of the flow, sometime dramatically, as, for example, in the reduction or suppression of unwanted small droplets in spraying. Understanding the interplay of flow and polymer microstructure in complex flows is key to designing and controlling important processes such as ink-jet printing, spraying, and coating. Much progress has been made recently towards understanding the dynamics of dilute polymer solutions in simple flows by visualizing directly polymer molecules (DNA) in simple shear and extension. Visualizing directly polymer molecules in free surface flows would promote similar progress by displaying how detailed flow features affect the polymer conformation, and by providing valuable information to test and validate, in realistic flows, models of the fluid dynamics of dilute polymer solutions.

In this study fluorescence microscopy of single DNA molecules is used to investigate the behavior of ultradilute polymer solutions in a small coating flow cell. In such ultradi-

[a)]Corresponding author; electronic mail: mp@rice.edu

lute solutions, the polymer molecules stretch and relax under combined action of the velocity gradient and intramolecular (elastic) and Brownian forces as if they were in dilute solutions; however, because the concentration of polymer molecules is so incredibly low, macroscopic flow is equivalent to that of a Newtonian fluid [Harrison *et al.* (1998)]. Thus, in ultradilute solutions it is possible to separate the effect of flow on the polymer microstructure from the converse effect of the polymer microstructure on the flow. Because of this feature, ultradilute solutions are key for testing in complex flows that are coarse-grained as well as microscopic models of polymer chains in dilute solutions: the flow can be calculated with certainty based on established Newtonian flow equations, and the spatial distribution of the polymer microstructure can be evaluated and compared with measurements.

This study has two major goals. First, to assess whether fluorescence microscopy of DNA could be used to track the microstructural evolution of polymer solutions in small scale-coating flows. [Preliminary studies were reported by Torazzi (1998) and by Pasquali (2000)]. This we do by using DNA as an elastic tracer in a Newtonian flow field and observing the molecular conformation. The second is to provide information about polymer conformation in regions of interest like the recirculation, separation surfaces, and menisci. Such experimental data on polymer conformation in different regions of the flow will provide guidance for developing and validating computational models, both continuum and microstructural. The success of this technique in ultradilute solutions could pave the way for studying flows where the microstructure affects the flow as, for example, in dilute, semidilute, and concentrated polymer solutions, entangled or not.

A. Free surface flows

Free surface flows arise when a flowing liquid layer meets another fluid (gas or liquid) and forms an interface. Examples of flows with free surfaces or free boundaries can be found in coatings, polymer processing, manufacturing processes (e.g., ink-jet printing), microfluidics (e.g., DNA arrays), and biology (e.g., deformation of blood cells, air displacement in pulmonary alveoli).

In coating processes, one or more thin layers of liquid are delivered to and deposited on a fast-moving web. The coating liquid is simultaneously sheared and extended, and often suffers strain reversal as it traverses the coating bead. Peak deformation rates are typically $10^4 - 10^5\ s^{-1}$ in shear and approximately one order of magnitude lower in extension. The polymer molecules in the coating liquid are distorted from their equilibrium conformation by the velocity gradient; this alters the behavior of the liquid, and affects the flow itself. Free surfaces, contact lines, boundary and internal layers, flow separations, and microrecirculations complicate coating flows. Experimental information on polymer microstructure in coating flows is needed to understand the flow behavior of polymer solutions and to guide and validate models of viscoelastic free surface flows.

Two methods are typically used to detect macromolecular conformation in polymer solutions, light scattering [Flory (1953), Chap. 7] and flow birefringence [Fuller (1995); Janeschitz-Kriegl (1983)]. The need to precisely measure scattered light over a wide range of angles around the sample makes light scattering a poor technique for studying complex free surface flows, where free surfaces and glass and metal walls reflect light which interferes with the scattering signal. The main hurdle in using birefringence to study coating flows is currently the lack of a water-based polymer solution with a stress-optical coefficient large enough to permit the detection of birefringence in dilute solutions. Moreover, light scattering and flow birefringence experiments do not provide direct measurement of polymer conformation.

Direct visualization of ordinary synthetic polymer molecules is difficult because their

small dimensions (10–100 nm) are well below the resolution of the best light microscopes (250 nm). DNA molecules behave qualitatively as long-chain ordinary synthetic polymers [Perkins *et al.* (1994a,b)] and can be dissolved in water. DNA molecules of appropriate length can be marked with fluorescent stains and visualized by optical microscopy; therefore, they constitute an attractive model system by which to study how polymer molecules deform in a coating bead. As new staining techniques develop, synthetic polymers will also lend themselves to single-molecule visualization studies, e.g., fluorescent ultrahigh molecular weight polyacrylamide [Wang *et al.* (2002)].

B. Visualization of flowing DNA molecules

Morikawa and Yanagida (1981) first visualized DNA molecules by fluorescence light microscopy. They used DAPI fluorescent stain and several different types of DNA, including T4 and λ DNA. The cross section of the DNA (2 nm) was well below the resolution of the optical microscope, so the DNA appeared more than 100 times thicker; however, the conformation of the stained molecules was clearly visible. Yanagida and Hiroaka (1983) showed that the instantaneous shape of equilibrated DNA molecules resembles an ellipsoid rather than a sphere. This has been confirmed recently by Haber *et al.* (2000).

Perkins *et al.* (1994b) used fluorescent DNA molecules in concentrated entangled aqueous solution to visualize reptating molecules and to measure the relaxation time of DNA molecules of different contour lengths [Perkins *et al.* (1994a)]. Although the images show directly only conformation of the DNA molecules, they provide information on the approximate location of active points of entanglement. Fluorescence microscopy of DNA was then used to study dilute DNA molecules in uniform flow [Perkins (1997); Perkins *et al.* (1995)], in planar extensional flow [Perkins (1997); Perkins *et al.* (1997, 1999); Smith (1999); Smith and Chu (1998)], in shear flow [Hur *et al.* (2001); Le Duc *et al.* (1999); Smith (1999); Smith *et al.* (1999)], and more recently in mixed flows [Babcock *et al.* (2003)] and in simple rectangular microchannels [Shrewsbury (2000); Shrewsbury *et al.* (2002, 2001)].

Both single-molecule conformation and average conformation of the flowing DNA provide important experimental information about the behavior of flowing linear polymers, and can be used to test the predictions of theoretical models of polymer dynamics in viscometric as well as complex flows. Larson *et al.* (1997, 1999), Hur *et al.* (2000, 2001), and Jendrejack *et al.* (2002) have been pioneers in the comparison between experiments and molecular models of DNA conformation in uniform flow, homogeneous extensional flow, and shear flow. Such modeling studies are now being extended to nonhomogeneous and confined flows [Chopra *et al.* (2003); Jendrejack *et al.* (2003, 2004); Woo *et al.* (2004a,b)].

C. Roll-knife coating

In a roll coating process a thin film is deposited on a continuous web using two or more rolls. The liquid is carried by one or both rolls into the gap between the rolls, and the film thickness and its uniformity on the web are controlled by the gap between the rolls and their relative speed. In knife coating, the liquid is metered by a rigid knife held close to the web. The excess coating liquid is metered by the knife and forms a thin coating on the continuous web. The film thickness depends on the width and the shape of the gap between the knife and the web [Coyle (1997)]. A roll-knife coating system combines the two coating processes: the roll feeds the liquid and the knife meters it and forms a film on the web. Here, we use a stationary glass plate next to a roll to create a

roll-knife coating process. The flat glass plate acts as a knife that meters the flow and allows optical access to the coating bead. Savage (1977), Bauman *et al.* (1982), Coyle *et al.* (1986), and Adachi *et al.* (1988) have used a plate-roll system and found that the stability and the behavior of the flow are similar to those of forward roll coating but the window of operation is smaller. Gaskell *et al.* (1998) measured the pressure profile in the coating bead at different roll speeds in a plate-roll apparatus. At low flow rates the pressure at the downstream free surface was greater than that at the upstream free surface, and the profile had a linear gradient similar to that in roll coating. They also confirmed the theoretical prediction that, upon an increase in flow rate the slope of the pressure curve decreases and has a local maximum (upstream of the minimum gap) and a local minimum (downstream of the minimum gap). This behavior is also observed in forward roll coating [Coyle *et al.* (1986); Greener and Middleman (1975)]. The coating bead can experience failure due to the hydrodynamics and elasticity of the coating liquid. ''Ribs'' with sinusoidally varying film thickness can appear across the coated web even in Newtonian liquids [Coyle (1997), and references therein] and are exacerbated by the presence of even minute quantities of high molecular weight flexible polymers [Dontula (1999)]; in this latter case, the ribs can develop into full septa. The occurrence of such ribs or septa destroys the uniformity of the coated film, which is an important requirement in industrial coatings.

II. EXPERIMENT

A. Apparatus

A small roll-and-knife coating flow cell was designed to fit under a microscope. The flow cell consisted of a steel roll of 12.7 mm diameter mounted on high precision ball bearings inside a 22 mm inner diameter (i.d.) steel tube [see Pasquali (2000); Torazzi (1998), for further details]. The top of the tube was cut off and a microscope coverslip (0.13 mm thick) was used to cover the cell (Fig. 1), leaving an adjustable gap of 25–60 μm between the top of the roll and the bottom of the coverslip. The gap was measured for each experiment. The bottom of the enclosing tube was flattened and mounted on an aluminum base. The steel roll was connected with a telescopic coupling to a AC high-resolution microstepping motor Compumotor S/SX 57-51 (Parker Hannifin Corporation, Compumotor Division, Rohnert Park, CA) mounted on an ordinary lab jack. The maximum angular velocity of the motor was 50 rps. Angular velocity of 0.01–0.5 rps was used in the study. The angular velocity and acceleration of the motor were controlled by a personal computer. The aluminum base was attached to the microscope xyz-positioning stage (Prior ProScan 0.1 μm resolution and 1 μm repeatability). Different regions of the flow were imaged by moving the flow cell with the positioning device.

The cell was filled with approximately 5 ml of liquid. A thin layer of liquid was picked up by the rotating roll and transferred to the coverslip, where it formed the coating bead (Fig. 1). The DNA in the coating bead was imaged from the top; therefore, the images of flowing DNA are two-dimensional projections on a horizontal plane of three-dimensional molecules that are sometimes stretched by the velocity gradient in a vertical plane and hence often straddle the plane of focus.

B. Materials

Fluorescently labeled λ-bacteriophage DNA was used as the model polymer. The DNA molecule (New England Biolabs Inc., Beverly, MA) has 48 502 base pairs and has a molecular weight of 31.5 Mg/mol. The DNA molecules were stained with the dye YOYO-1 (Molecular Probes Inc., Eugene, OR) at a 1:4 dye-to-base pair ratio. At this

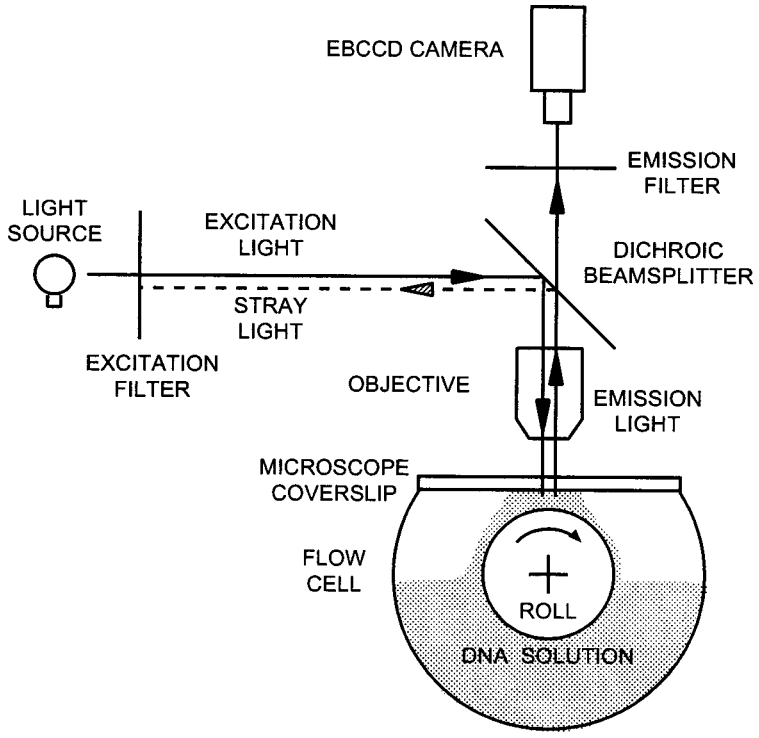

FIG. 1. Schematic of the roll-and-knife coating flow cell and epifluorescence microscopy setup used to visualize stained DNA molecules in the coating flow cell.

staining ratio a DNA molecule has a contour length of 22 μm [Perkins (1997)]. The persistence length is $\sim$ 70 nm (5 mM NaCl) and its hydrodynamic diameter is $\sim$ 2 nm [Hagerman (1988); Kam *et al.* (1981)].

A stock solution with DNA concentration 0.65 μg/ml was prepared in a TRIS-borate EDTA (TBE) buffer. The stock DNA was diluted and suspended in high viscosity ($\sim$ 40 and $\sim$ 100 mPa s) sugar solutions. The viscosity of the solution was measured using a strain controlled rheometer ARES 100 FRT (Rheometrics Scientific Inc., Piscataway, NJ). The measurements were done in Couette geometry (bob diameter = 32 mm, cup diameter = 34 mm). The dimensionless flow numbers were based on the viscosity of each microscopy solution. The DNA concentration in the coating liquids was well below the overlap concentration ($10^{-5}c^*, c^* \approx 37\,\mu$g/ml). At this concentration the DNA molecules are always well spaced (approximately three to four molecules in the field of view); thus, single molecules can be visualized. Because of the large molecular spacing, the DNA molecules behaved as isolated coils in the dilute liquids. A buffer solution was prepared by diluting to 50% TBE buffer (Sigma Chemical Co., St. Louis, MO) in deionized water, with 5 mM NaCl and 1 vol % 2-mercaptoethanol (Sigma Chemical Co., St. Louis, MO). Mercaptoethanol slows photobleaching of the dye by scavenging free oxygen [Yanagida *et al.* (1983)]. Sugar solutions, $\sim$ 40–45 wt % sucrose and $\sim$ 20 wt % glucose, prepared in the buffer, were used to enhance the viscosity of the DNA solutions. The static contact angle between the 41 mPa s ($\sim$ 60 wt % sugar) solution and the coverslip was measured to be 35.5° by video imaging of liquid drops on the glass surface.

The relaxation times of λ DNA were determined using the data of Perkins *et al.* (1997), who reported that the relaxation time of λ DNA in a 41 mPa s solution of water

and sugar is 3.9 s. The relaxation time of λ DNA is proportional to the viscosity of the solution [Smith and Chu (1998)]; thus in our experiments with dilute solutions of viscosity 40 and 100 mPa s, the relaxation times were approximately 3.9 and 10 s, respectively.

C. Fluorescence microscopy setup

Visualization experiments were performed with a Nikon Eclipse E600 epifluorescence microscope equipped with a 100 W mercury lamp and a Nikon Plan-Apo oil immersion objective with 60× magnification and 1.4 numerical aperture.

YOYO-1 bound to DNA has an absorption peak at 491 nm and an emission peak at 509 nm [Haugland (1996)]. The filter set XF100-2 (Omega Optical, Brattleboro, VT), used to image stained DNA included a band pass excitation filter (450–500 nm), a dichroic mirror (500 nm cutoff) and a long pass emission filter (520–560 nm).

Images of flowing DNA were collected at 30 frames per second with an electron bombarded charge coupled device (EBCCD) camera, model C7190 (Hamamatsu Photonics, Hamamatsu-City, Japan) controlled by the software METAMORPH (Universal Imaging Inc. Downigtown, PA). The images were acquired directly on a PC through METAMORPH. Streak-free images of fast-moving molecules ($\sim 100\ \mu$m/s) were obtained by de-interlacing the video camera output, i.e., the video output was split into frames corresponding to odd and even scan lines and missing alternate lines were filled with previous scan lines.

III. RESULTS AND DISCUSSION

We use two dimensionless numbers to describe the intensity of the flow. A local Weissenberg number $Wi \equiv \lambda\dot{\gamma}$, where λ is the relaxation time of the DNA, and $\dot{\gamma}$ is the local strain rate and a characteristic Weissenberg number $Wi^e \equiv \lambda v/h$, where v is the roll speed and h is the minimum gap between the glass coverslip and the roll. The local strain rate is defined as $\dot{\gamma} \equiv \sqrt{|\Pi_{2\mathbf{D}}|}$, where $\mathbf{D}$ is the rate of strain (the symmetric part of the gradient of velocity) and Π_{2D} is the second invariant of $2\mathbf{D}$. In the experiments described here in Sec. III, Wi^e ranged from 38 to 3500, the Reynolds number $Re \equiv \rho v h/\mu$ ranged from 4.4×10^{-4} to 2.5×10^{-2}, and the capillary number $Ca \equiv \mu v/\sigma$ was 2×10^{-4}–3×10^{-2}. The ratio of the gap to the roll radius ranged from 4.2×10^{-3} to 8.9×10^{-3}.

The Deborah number in this flow is $De \equiv \lambda/t_r = \lambda v/L$, where t_r is the average time of residence of the liquid in the bead computed by the roll's tangential velocity v and bead length L; the Deborah number is related to the Weissenberg number through the ratio of gap width to bead length, $De = Wi^e h/L$. The length of the bead ranged from approximately 5 to 8 mm, depending on the viscosity of the liquid and the roll's speed; therefore, the Deborah number in the flow was approximately two orders of magnitude lower than the Weissenberg number.

A. Low capillary number flow

The liquid layer picked up by the rotating roll was thinner than the gap between the coverslip and the top of the roll when the roll velocity was lower than a critical velocity. Wilson (1982) showed that the film thickness at the top of a roll dragging liquid out of a pool is

$$H \sim \frac{(\mu\omega)^{2/3}}{(\rho g)^{1/2}\sigma^{1/6}(1-\cos\theta)^{1/2}}, \tag{1}$$

TABLE I. Location of image planes (depth) at the minimum gap position for various local Weissenberg numbers and experimental conditions.

Experiment	Wi	y (μm)	Minimum gap (μm)	Film thickness, H (μm)	Roll speed (rps)	Viscosity (mPa s)
E1	84	30	41.7	7.8	0.01	41
E2	106	32.9	42.1	8.1	0.01	43
E3	147	31.8	55.5	18.7	0.015	103
E4	176	3.3	35.3	23.6	0.05	44
E5	195	16.6	35.3	22.4	0.05	41
E6	217	26.3	45.8	22.5	0.02	103
E7	302	25.4	45.8	29.3	0.03	103
E8	361	21.8	35.3	23.6	0.05	44

where μ is the solution viscosity, ω is the roll speed, ρ is the density of the solution, σ is the surface tension, and θ is the angle up to which the roll dips in the liquid pool. In our experiments $\theta = 90°$, i.e., the roll is half submerged in the liquid pool. Table I lists the film thickness [computed with Eq. (1)] in each of the experiments performed. In all the experiments in this velocity range (capillary number) the minimum gap is greater than the calculated film thickness; thus, the coating bead was established by depositing a drop of liquid on the roll surface before the coverslip was placed on the device. The capillary pressure across the free surfaces dominates the viscous pressure and causes backflow under the coverslip. A large recirculation is present under the coverslip [Figs. 2(a) and 2(b)]. Images were acquired in different planes along the optical axis at the position of the minimum gap between the roll and the glass bar. To minimize edge effects the molecules were visualized in the middle of the flow cell equidistant from the two bearings.

1. Flow under the coverslip

The DNA molecules were nearly stationary close to the coverslip. As the focal plane was lowered toward the roll, the DNA moved opposite to the roll with growing velocity initially, then more slowly until a plane was found where the DNA was nearly stationary. As the focus was lowered further, the DNA moved with growing velocity in the same direction as the roll. The velocity profile in the gap can be estimated by lubrication approximation with a no-slip boundary condition at the bottom of the coverslip and at the top of the roller,

$$v(x,y) = 3\omega R\left(1-\frac{x^2}{2R^2}\right)\frac{y^2}{h(x)^2}-\frac{6Q}{h(x)^3}y^2+\frac{6Q}{h(x)^2}y-2\omega R\left(1-\frac{x^2}{2R^2}\right)\frac{y}{h(x)}, \qquad (2)$$

where $y = 0$ is the bottom of the coverslip and $y = h(x)$ is the roll, ω is the roll speed, $x = 0$ is the minimum gap position, and Q is the flow rate per unit width (Fig. 2). Q was calculated by measuring the position of the zero velocity plane at $x = 0$. Figure 2(b) shows the streamlines computed by the Galerkin finite element [Pasquali (2000)] using appropriate boundary conditions. [Supplementary Fig. S1 (see the reference section for an EPAPS document), compares the location of the zero velocity plane measured experimentally and that computed from finite element solution. Mesh convergence is shown by plotting profiles computed with two different meshes.]

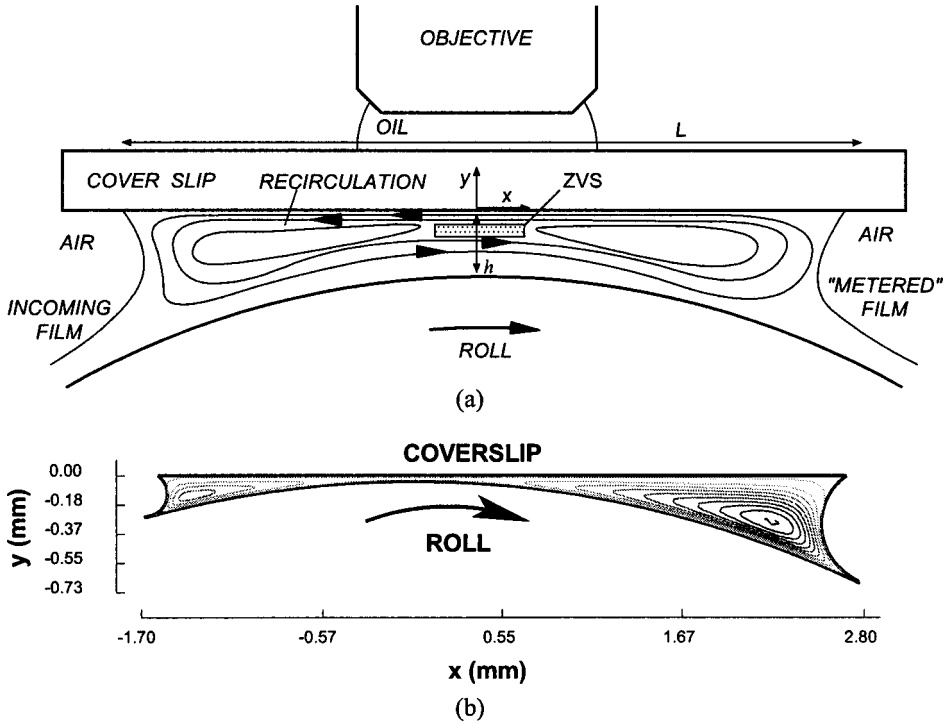

FIG. 2. (a) Schematic of the flow at low roll velocity. The zero velocity surface (ZVS) is shaded. Images of flowing DNA molecules were captured in different planes at the position of the minimum gap between the coverslip and the roll. (b) Streamlines computed with the Galerkin finite element solution of flow equations at low roll speed (to scale). The computational domain extends further upstream and downstream than shown here.

[At the two solid boundaries (coverslip and roll), no slip and no penetration are imposed. The flow rate Q is unknown; hence inflow is treated as a free boundary and the so-called ''free boundary condition'' is imposed there [Carvalho (1996); Papanastasiou *et al.* (1992)]. Fully developed flow is imposed at the outflow. At the free surface, force balance and a kinematic boundary condition are imposed [see Pasquali (2000); Pasquali and Scriven (2002) for details]. The position of the static contact line along the coverslip is not fixed; the static contact angle of the sugar solution on the glass coverslip is imposed at the line of contact.]

Schunk and Scriven (1990) have modeled complex mixed extensional and shear flows based on the flow classification criterion of Astarita (1979) using the frame invariant quantities $\mathbf{D}$, the rate of strain, and $\mathbf{w}_{\text{rel}}$, the relative rate of rotation of the unit eigenvectors $\mathbf{e}_i$ of $\mathbf{D}$ with respect to the vorticity,

$$\mathbf{D} \equiv \tfrac{1}{2}(\nabla\mathbf{v}+\nabla\mathbf{v}^T) \tag{3}$$

$$\mathbf{w}_{\text{rel}} \equiv \mathbf{e}_i\times\left(\frac{\partial\mathbf{e}_i}{\partial t}+\mathbf{v}\cdot\nabla\mathbf{e}_i\right)-\frac{1}{2}\nabla\times\mathbf{v}. \tag{4}$$

The flow is pure shear when $\|\mathbf{w}_{\text{rel}}\|/S = 1$ and pure extension when $\|\mathbf{w}_{\text{rel}}\|/S = 0$, $S = \sqrt{\|\Pi_{\mathbf{D}}\|}$.

Planes with different velocity gradients ($\sqrt{|\Pi_{2\mathbf{D}}(x,z)|}$) were chosen to investigate molecular conformations in a range of local Weissenberg numbers. Figure 3 shows the

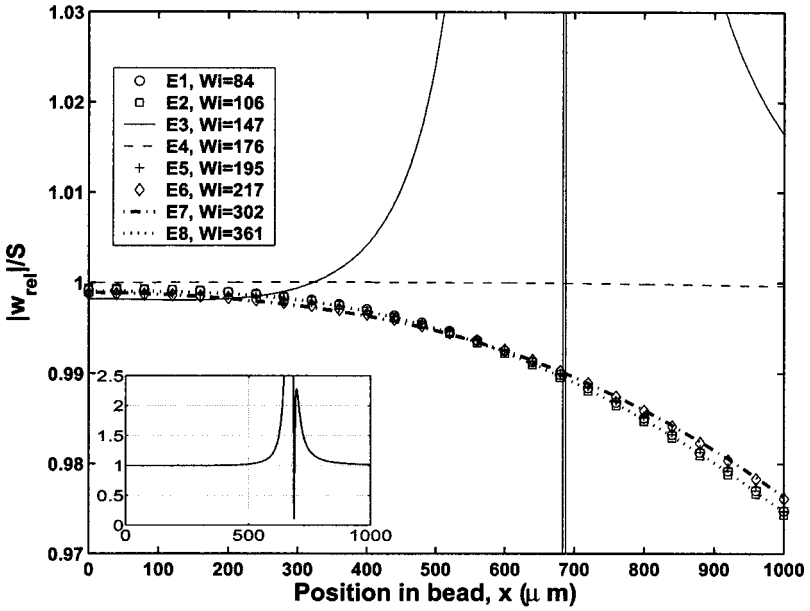

FIG. 3. Flow strength parameter $\|\mathbf{w}_{\mathrm{rel}}\|/S$ as a function of the position in the coating bead at different depths that correspond to local Weissenberg numbers. The minimum gap position is at $x = 0$. The inset shows the flow strength parameter for experiment E3.

flow strength parameter ($\|\mathbf{w}_{\mathrm{rel}}\|/S$) as a function of position x in the coating bead on streamlines that correspond to the image planes. Near the minimum gap position (400 μm on either side) clearly the flow is shear dominated ($\|\mathbf{w}_{\mathrm{rel}}\|/S-1 \lesssim 3\times10^{-3}$). In experiment E3, the velocity gradient nearly vanishes at $x \sim 680\,\mu$m; there the flow changes rapidly from shear dominated, to almost purely rotational ($\|\mathbf{w}_{\mathrm{rel}}\|/S \gg 1$), to extensional ($\|\mathbf{w}_{\mathrm{rel}}\|/S \approx 0$), back to shear dominated.

In the zero velocity plane molecules were observed stretching in the direction of the velocity (and possibly of the velocity gradient), whereas no change in size in the direction of the vorticity could be detected (supplementary Fig. S2; see the reference section for an EPAPS document). The zero velocity plane moved closer to the coverslip as the roll velocity was increased.

Images of molecules moving at high speed ($\sim$ 100–230 μm/s) were deinterlaced to reduce streaking and processed frame by frame in an image analysis program written in MATLAB. The major and minor axes of the ellipses of the equivalent second moment were computed for each molecule. Molecular extension was measured as the maximum distance between the two farthest points on the molecule. One to two thousand measurements were made at each local Weissenberg number.

Figure 4(a) shows the mean fractional extension of DNA at the minimum gap. As expected, polymer extension increases with the Weissenberg number due to higher hydrodynamic drag experienced across the molecule. The extension measured at low Wi agrees well with the results of Smith *et al.* (1999). The mean fractional extension grows gradually and asymptotes to 0.5, confirming the trend previously reported in experiments [Smith *et al.* (1999)] and in simulations of Kramers chains [Hur *et al.* (2000)] in shear flow. Figure 5 shows the distributions of fractional extension at different local Weissenberg numbers. The distributions become broader with an increase of Wi. In shear, the rotational component of the flow destabilizes the extended molecule, which rotates and

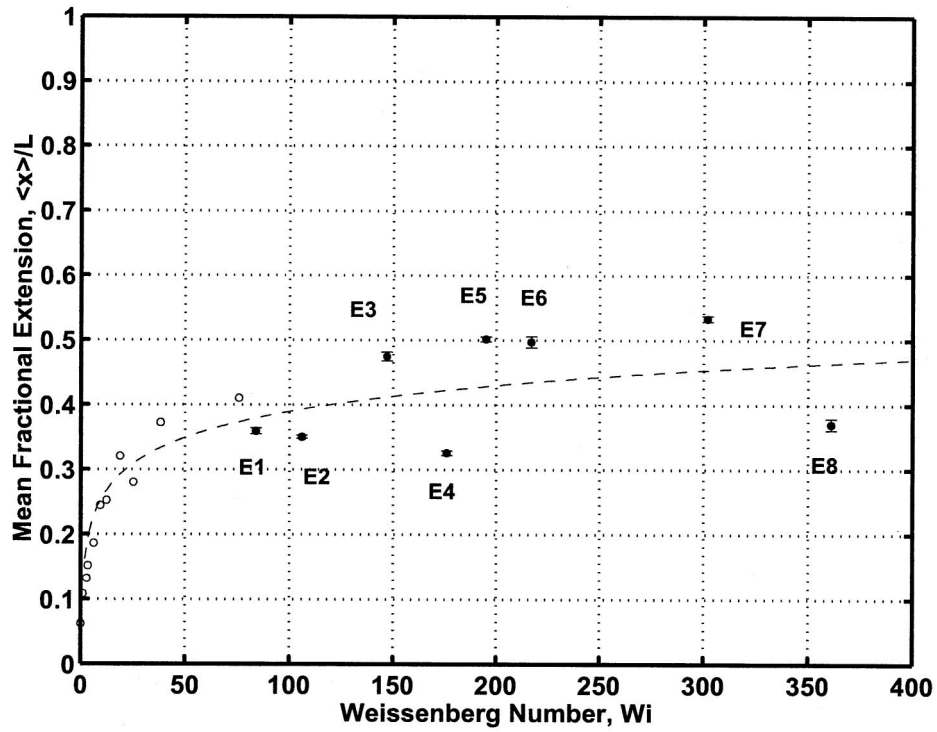

(a)

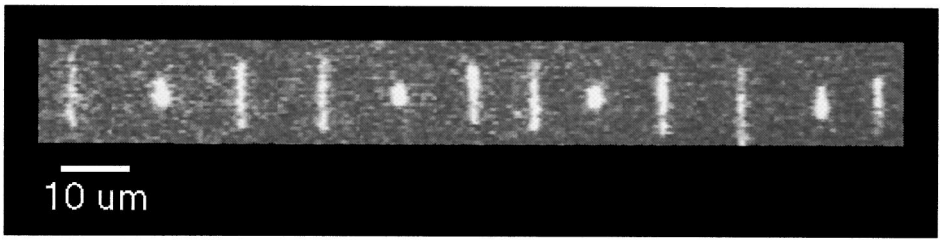

(b)

FIG. 4. (a) Mean fractional extension of molecules in pure shear flow at the minimum gap location (closed symbols). The mean extension asymptotes to 0.5 at high Wi and agrees with the data on pure shear of Smith *et al.* (1999) (open symbols). The line is a guide to the eye and the error bars are standard errors. (b) Molecule undergoing oscillations from extended to coiled conformation (yoyo motion) for local $Wi = 361$. The snapshots are at intervals of 1/30 s.

folds back into a coiled conformation. The molecules fluctuate from an extended state to a coiled state and back into an extended state like a yoyo [Fig. 4(b)]. With an increase of Wi the molecules experience higher extension while fluctuating between extended and coiled states. The fluctuations in extension were measured to be 13%–28% the contour length. At high Weissenberg numbers the probability of finding all lengths becomes equal [Hur *et al.* (2000)]. The minimum measured extension is close to the equilibrium size of the molecule (~ 1.5 μm). Some measurements ($< 1.5\%$) were 1–2 μm above the contour length of a DNA molecule because of small errors introduced by the image thresholding algorithm.

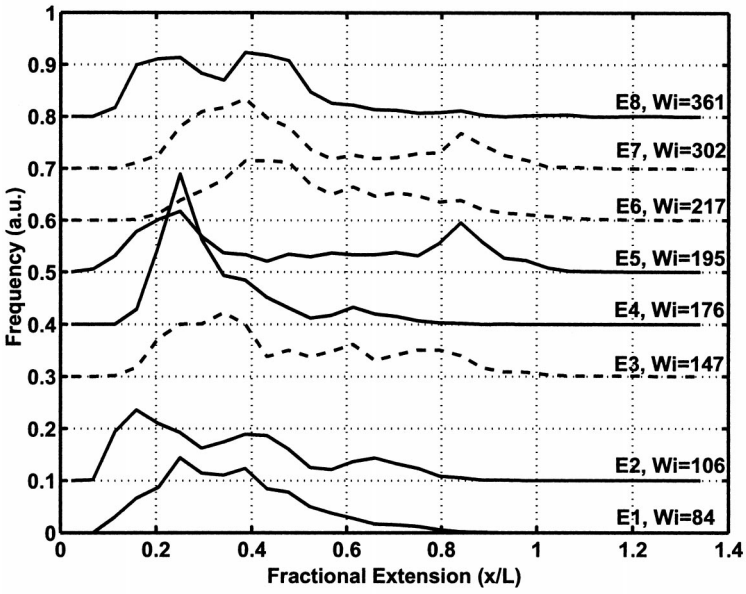

FIG. 5. Probability distribution of molecular extension in the shear flow region at the minimum gap position for different values of local Wi. 1 μm bins are used to calculate the histograms which are offset from zero for clarity. Solid and dashed lines represent distributions obtained with $\mu \sim 40$ and 103 mPa s solutions, respectively.

Figure 6 shows the average shape and orientation of the DNA in the flowing dilute solutions under shear flow. The size and orientation were obtained by calculating the ellipse with second moment equal to that of the image [two-dimensional (2D) projection] of the molecule. The orientation of the average conformations shows that the molecules are completely aligned with the velocity direction. The stretch along the velocity direc-

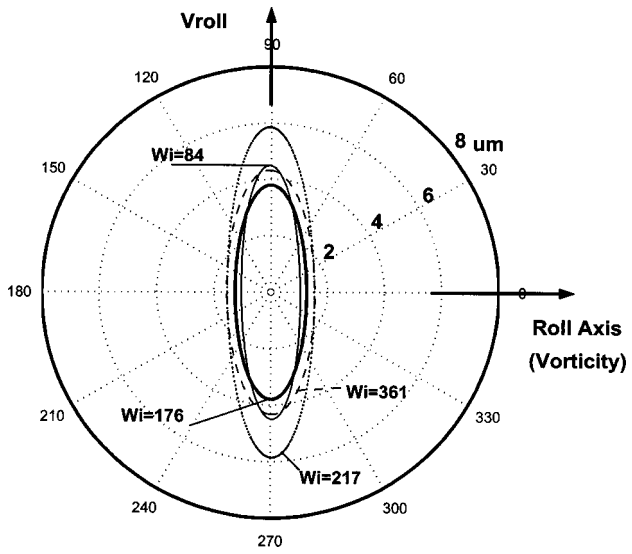

FIG. 6. In-plane average conformation of DNA in shear flow computed with the ellipsoid approximation.

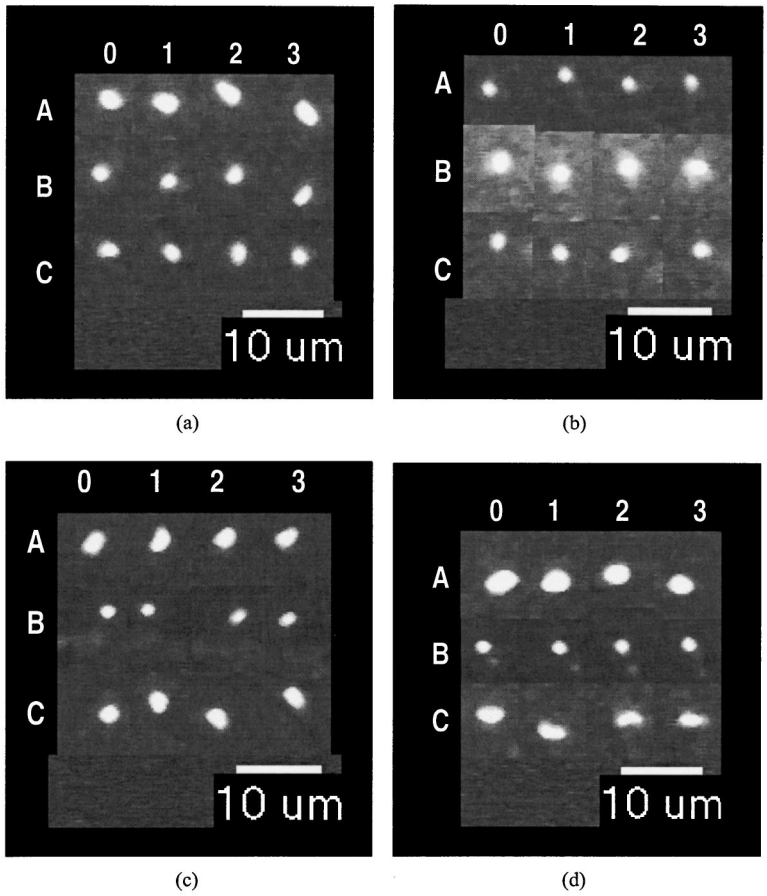

FIG. 7. Images of DNA molecules near contact lines. The images of the three molecules (A,B,C) are at 1 s intervals. (a) Near upstream meniscus (6 μm below the coverslip), $Wi^e = 38$; (b) near upstream meniscus (12 μm below the coverslip), $Wi^e = 194$; (c) near downstream meniscus (1.5 μm below the coverslip), $Wi^e = 44$; (d) near downstream meniscus (1.6 μm below the coverslip), $Wi^e = 247$.

tion increases and plateaus with an increase of local Weissenberg number. The spanwise dimension (along the roll axis) does not change considerably with the local Weissenberg number, in agreement with the results of Smith *et al.* (1999).

2. Flow near contact lines

Very few molecules were found at the menisci just below the coverslip, either upstream or downstream of the minimum gap position, even when the concentration of DNA in these solutions was raised to $10^{-4}c^*$. Near the contact lines, the molecules remain coiled as they traverse the field of view at very low axial velocity. Figure 7 shows images of molecules taken at 1 s intervals at two different characteristic Wi^e at the upstream and downstream menisci. The velocity gradient close to the contact lines appears to be too weak to stretch the DNA even though the characteristic Weissenberg number of the flow is high (38–247). This may be due to the acute contact angle (the liquid wets the coverslip) at the free surface, which leads to trapping of molecules. These molecules have a high residence time in this region.

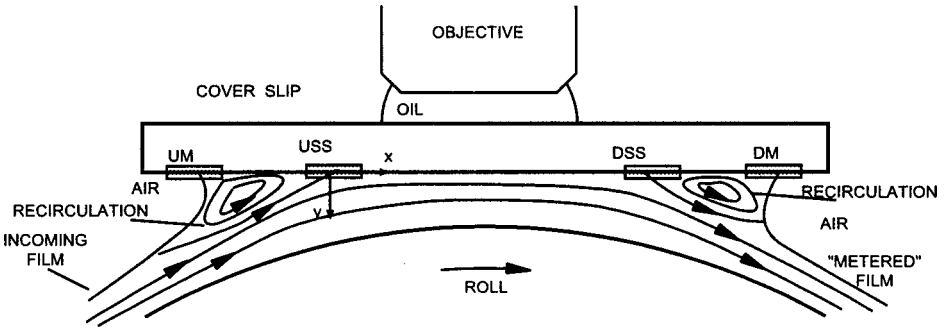

FIG. 8. Diagram of the flow at high roll velocity. The locations of the visualized regions are shaded: USS—upstream separation surface; DSS—downstream separation surface; UM—upstream meniscus; DM—downstream meniscus. The diagram is not to scale; the gap is really much narrower, and the separation lines are really much closer to the location of the minimum gap.

B. High capillary number flow

At high roll speeds (high capillary number), the capillary pressure across the two free surfaces is not high enough with respect to viscous forces to cause backflow. The big recirculation under the coverslip, present at low roll velocity, breaks into two smaller recirculations near the upstream and downstream menisci (Fig. 8). As the capillary number is increased further, the layer picked up by the roll is thicker than the gap; part of it is rejected by the metering action of the coverslip, and eventually a backflow of liquid arises from the coating bead to the pan.

Images were acquired at the upstream and downstream menisci, at the upstream separation surface that demarks the boundary between recirculating liquid and metered liquid, and at the downstream separation surface between the metered liquid and recirculation at the downstream meniscus. The menisci were located by focusing the objective immediately under the coverslip inside the coating bead, then moving the microscope stage horizontally until a dark region with no DNA molecules appeared. The separation surfaces were found by focusing the objective under the coverslip inside the coating bead, then moving the microscope stage horizontally until a region was found with some DNA molecules moving with the roll and others moving opposite the roll. Deeper regions of separation surfaces were found by repeatedly slightly lowering the focal plane and adjusting the horizontal position to keep the separation surface in the center of the field of view.

1. Upstream separation surface

The upstream separation surface was 1.1 ± 0.05 and 1.4 ± 0.05 mm upstream of the location of the minimum gap in experiments at average $\langle Wi\rangle = 240\,(Ca = 0.009)$ and 265 $(Ca = 0.027)$, respectively. The sequence of images in Fig. 9 was taken at characteristic $Wi^e = 2031\,(\langle Wi\rangle = 240)$. The molecules are moving toward the coverslip. The separation surface is marked in the four images. The molecule above the upstream separation surface (A) moves against the roll (bottom to top) and is in the recirculating liquid. The molecule below the upstream separation surface (B) is in the metered liquid and moves with the roll (top to bottom). The final snapshot shows a molecule (C) that comes into focus stretched at the upstream separation surface.

The DNA molecules in Fig. 9 lie mainly in the plane of focus. Near the separation surface by the stagnation line the flow is chiefly extensional; the principal direction of extension of the rate of strain is essentially parallel to the coverslip, and the principal

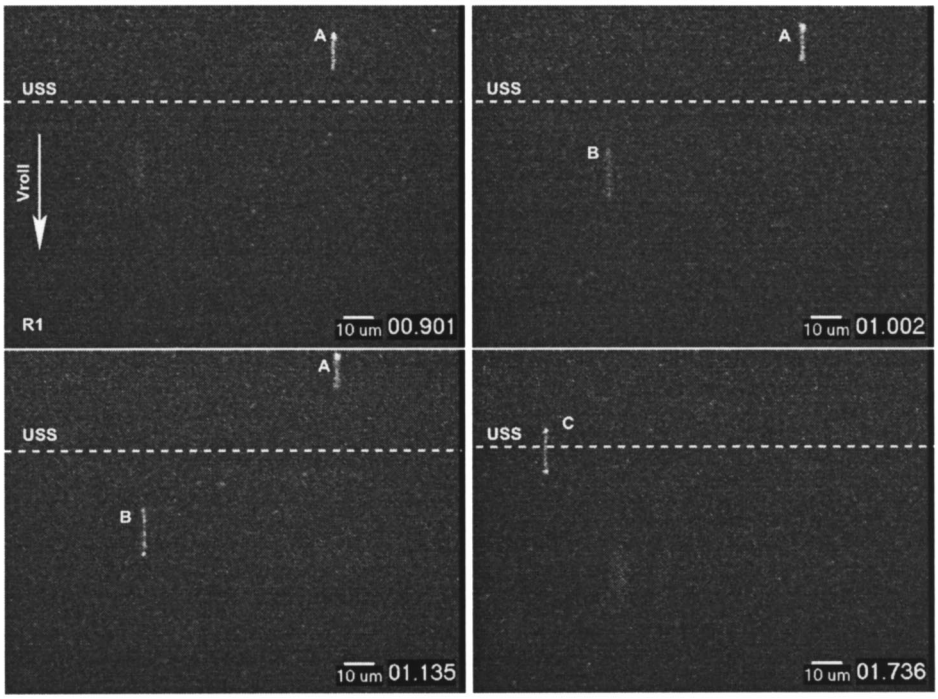

FIG. 9. Molecules moving with and against the roll at the upstream separation surface (USS) in high capillary number flow with characteristic $Wi^e = 2031$. Molecule A moves against the roll (bottom to top) and is in the recirculating liquid. B moves with the roll (top to bottom) and is in the metered liquid. Both A and B move away from the USS as they move toward the glass coverslip. Molecule C comes into focus stretched right at the USS.

direction of compression is normal to the coverslip, and the DNA tends to align along the principal direction of extension.

The stagnation flow at the separation surface (near the coverslip) can be described by the stream function [Batchelor (1967)],

$$\psi(x,y) = Ay^2x \sin\theta_0 - Ay^3 \cos\theta_0. \tag{5}$$

Here, $(x,y) = (0,0)$ is the point of stagnation on the coverslip and x and y are coordinates parallel and perpendicular to the coverslip (Fig. 8). The stagnation line forms an angle θ_0 with the coverslip. An approximate value of θ_0 was measured by moving the stage horizontally (along x) to position the upstream separation surface in the middle of the field of view at different depths (y). The characteristic flow number in the field of view is best given as the average over the imaging volume (volume formed by the field of view and the depth of field) $\langle Wi \rangle \equiv \lambda \int_V \sqrt{\|\Pi_{2\mathbf{D}}\|}\, dV$.

We observed molecular conformation in two flows with $\langle \|\mathbf{w}_{\text{rel}}\|/S \rangle = 0.3728$ ($y = 3.6\,\mu$m, $\theta_0 = 3.4°$) and $\langle \|\mathbf{w}_{\text{rel}}\|/S \rangle = 0.4137$ ($y = 6.3\,\mu$m, $\theta_0 = 4.6°$), and average $\langle W_i \rangle = 240$ and 265, respectively. The molecules moved at speeds of ~ 10–12 μm/s toward the glass slide and stayed in the field of view for a few frames.

Figure 10(a) shows the distributions of extensions measured at the two average $\langle W_i \rangle$. The two distributions are qualitatively similar, with a large number of measurements near full extension. Various molecular conformations were observed which had been reported previously in pure extensional flow [Perkins *et al.* (1997)]: folded, half-dumbbell (mol-

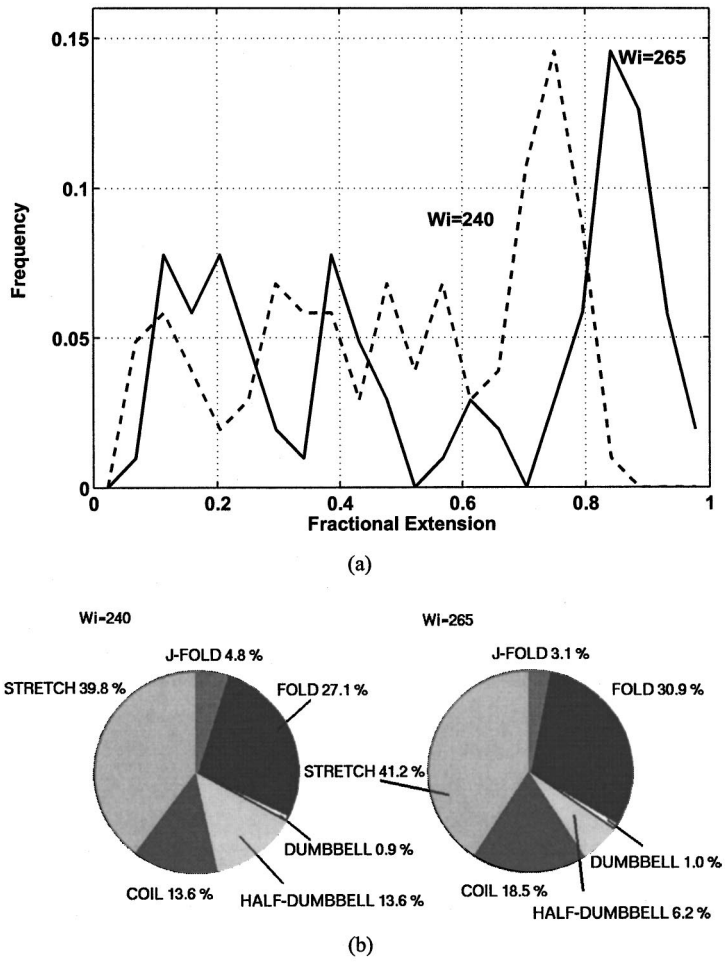

FIG. 10. (a) Measured distribution of fractional extension at the upstream separation surface for $\langle \|\mathbf{w}_{\text{rel}}\|/\|S\| \rangle = 0.3728$, $\langle Wi \rangle = 240$ (dashed line) and $\langle \|\mathbf{w}_{\text{rel}}\|/\|S\| \rangle = 0.4137$, $\langle Wi \rangle = 265$ (solid line). (b) Distribution of polymer conformations at the upstream separation surface at $\langle Wi \rangle = 240$ (left) and 265 (right).

ecule A in Fig. 9), stretched (molecule B in Fig. 9), and dumbbell (molecule C in Fig. 9) conformation were observed [Fig. 10(b)]. The mean fractional extension increases with the Weissenberg number and is $50\pm3\%$ and $56\pm3\%$ for average $\langle Wi \rangle = 240$ and 265, respectively. The major peak, corresponding to stretched molecules, is at fractional extension of 0.76 ± 0.03 for average $\langle Wi \rangle = 240$ and at 0.85 ± 0.01 for average $\langle Wi \rangle = 265$ (the distributions were fitted with four Gaussians for the four major conformations observed). The extension that the molecules experience is lower than the expected value of about 90% observed in steady mixed flow studies by Babcock *et al.* (2003). The extension is lower because the molecules experience strain $\dot{\epsilon} t_{\text{res}} \sim 1$ as they traverse the stagnation flow. At such small strain, many molecules are still stretching and have not reached steady state extension. This can also be seen in the probability distributions which resemble a combination of distributions of molecules with different residence times in purely extensional flow [Perkins *et al.* (1997)]. In the work of Perkins *et al.*'s work, the primary peak corresponding to stretched conformations grows as the residence

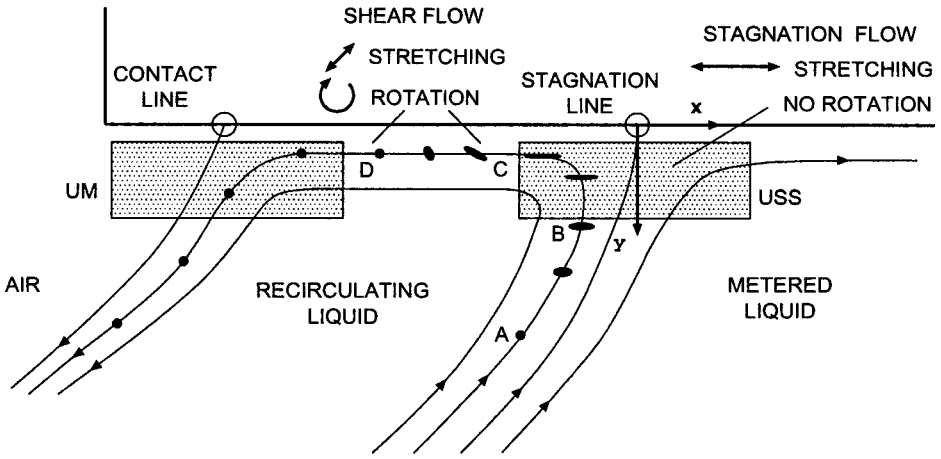

FIG. 11. Schematic of paths of DNA molecules between the upstream stagnation line (USS) and the upstream meniscus (UM). The DNA approaches the stagnation region at the USS in a nearly coiled conformation (A), then stretches approximately parallel to the coverslip as it traverses the stagnation region (B). In the shear-dominated velocity field it rotates and relaxes (C) as it moves towards the free surface. Due to the axial flow observed at the meniscus we cannot safely comment about conformation D. In flow without nodal recirculation the DNA would completely recoil (D) by the time it reaches the upstream meniscus. Not drawn to scale.

time of the molecules in the flow increases, while the secondary peaks (folded and coiled conformations) diminish as the molecules reach steady state extension. In our experiments we find peaks corresponding to stretched, folded, and coiled conformations, implying that not all the molecules have reached steady state extension.

2. Downstream separation surface

The DNA enters the stagnation flow region in a distorted conformation and then stretches along the streamline into the focal plane. The principal direction of extension is into the field of view, and the principal direction of compression is in the plane of focus; therefore, the DNA aligns predominantly along the optical axis as it approaches the separation surface. The DNA goes into the plane of focus as it nears the separation surface; thus, the images in Fig. S3 (see the Supplementary Material in the EPAPS document in the reference section for details) (frames 3–4) are projections of the shape of the molecule onto the field of view. Molecules that are extended along the objective axis as well as undistorted molecules give circular images; therefore, it is not possible to determine whether the molecules imaged at the downstream separation surface are coiled or partially stretched along the objective axis. For this reason, the distribution of measured molecular extension is not quantified here.

3. Upstream and downstream menisci

The DNA molecules near the upstream meniscus arrive from the upstream separation surface (Fig. 11), where they are stretched by extension dominated flow near the stagnation line. The molecules then traverse a region of slow, shear-dominated flow below the coverslip, where the velocity gradient has a large rotational component and a stretching component too weak to further extend the molecules. The DNA molecules therefore start to relax before reaching the upstream meniscus. Molecular relaxation at and near the free surface was not observed in our experiments due to the presence of nodal recirculation

(along the roll axis) in which extended molecules were observed to move axially. Figure S4 (see Supplementary Material in the EPAPS document in the reference section) shows a typical DNA molecule at the upstream meniscus at $Wi^e = 2031$ and $Ca = 0.009$. The molecule is moving axially and, unexpectedly, is strongly extended axially.

Using a low magnification (10×) and long working distance objective we investigated the flow near the contact line to determine if the axial motion is due to the presence of ribbing instability. The contact line was observed to remain straight and stationary. The free surface below the contact line was wavy and was oscillating at ~ 1 Hz. At the gap to radius ratio in our experiments the critical capillary number for the onset of ribbing instability computed by stability analysis of simplified lubrication flow [Savage (1984)] is ~ 0.1 and that from experiments [Adachi *et al.* (1988)] is ~ 0.14. This is approximately 10 times higher than the capillary number in our experiments ($Ca = 0.009$). Coyle *et al.* (1990) showed that in symmetric forward roll coating flows the critical value of the capillary number was sensitive to the detection technique: by using a sensitive low angle reflection technique they found that ribbing instability set in at a capillary number that was five times lower than what had been established previously by naked-eye measurements [Greener *et al.* (1980); Pitts and Greiller (1961)]. Thus, it is possible that in a plate-roll system ribbing instability occurs at a lower capillary number than previously measured.

At the downstream contact line extended molecules were also observed to be moving axially (supplementary Fig. S5; see Supplementary Material in the EPAPS document in the reference section for details). But molecules were expected to be moving slowly and be mostly coiled close to the downstream meniscus even at a high Weissenberg number, because slow recirculation is present near the free surface. Interestingly, the gradients present due to the slow nodal recirculation are strong enough to stretch the molecules along the velocity direction as they move across the field of view.

The DNA molecules leave the region of the downstream meniscus in a slightly distorted conformation, traverse a region of shear-dominated flow under the coverslip where little stretching occurs, and reach the downstream separation surface in a conformation that is slightly extended along the flow direction.

IV. CONCLUSIONS

This work showed that single molecule visualization of DNA using fluorescence microscopy is a viable useful technique by which to investigate the behavior of ultradilute polymer solutions in scaled-down process flows. We investigated how linear polymer chains stretch and orient in a small roll and knife coating flow. We provided data on molecular conformation obtained in a flow which is more complex than the spatially homogeneous flows which have been reported in the literature so far. At low speeds, large recirculation was present below the coverslip; at the minimum gap, where the molecules experience shear flow, the mean fractional extension increases with the local Weissenberg number and asymptotes to 0.5, in agreement with previous results for homogeneous shear by Chu and co-workers, extended here to $Wi \sim 350$. At high roll speeds the molecules experience extension-dominated flow at the two separation surfaces. Interestingly, weak axial flow was present near the contact lines at a capillary number one order of magnitude lower than the critical value given in the literature for the onset of ribbing; the DNA molecules stretched axially there. The optical axis here was aligned with the velocity gradient and hence in certain regions the DNA straddled the focal plane; clearer images may be obtained in the future by aligning the optical axis of the microscope with the vorticity.

The results provided here give researchers who are trying to model DNA and polymers in general an opportunity to check whether the models which have been developed and tested in homogeneous flows do well enough in more complex flows (e.g., coating flows). Because we used ultradilute solutions (Newtonian solutions) the models of the polymer dynamics can be tested independently of the model of the coupling of the stress to the polymer conformation. Validating and testing models in an ultradilute regime, where the DNA does not affect the flow field, is the first step towards studying fully coupled problems where the DNA concentration is higher and the molecules affect the flow regime.

ACKNOWLEDGMENTS

The authors would like to thank L. E. Scriven, W. J. Suszynski, R. Torazzi, M. Montminy, C. K. Smith, J. Pierce, D. E. Smith, and G. J. Hirasaki. This work was supported by the National Science Foundation through Grant No. CTS-CAREER 0134389 and by the NSF Center for Biological and Environmental Nanotechnology (Grant No. EEC-0118007). Computational resources were provided by the Rice Terascale Cluster funded by NSF under Grant No. EIA-0216467 and by Intel and Hewlett Packard.

References

See **EPAPS** Document No. E-JORHD2-48-012404 for supplementary Figs. S1–S5. This document may be retrieved via the EPAPS homepage (http://www.aip.org/pubservs/epaps.html) or from ftp.aip.org in the directory directory/epaps/. See the EPAPS homepage for more information.

Adachi, K., T. Tamura, and R. Nakamura, ''Coating flow in a nip region and various critical phenomena,'' AIChE J. **34**, 456–464 (1988).

Astarita, G., ''Objective and generally applicable criteria for flow classification,'' J. Non-Newtonian Fluid Mech. **6**, 69–76 (1979).

Babcock, H. P., R. E. Teixeira, J. S. Hur, E. S. G. Shaqfeh, and S. Chu, ''Visualization of molecular fluctuations near the critical point of the coil-stretch transition in polymer elongation,'' Macromolecules **36**, 4544–4548 (2003).

Batchelor, G. K., *An Introduction to Fluid Mechanics*, 1st ed. (Cambridge University Press, New York, 1967).

Bauman, T., T. Sullivan, and S. Middleman, ''Ribbing instability in coating flows—Effect of polymer additives,'' Chem. Eng. Commun. **14**, 35–46 (1982).

Carvalho, M. S., ''Roll coating flows in rigid and deformable gaps,'' Ph.D. thesis, University of Minnesota, Minneapolis, MN, 1996; available from UMI, Ann Arbor, MI, Order No. 9621887.

Chopra, M., L. Li, H. Hu, M. A. Burns, and R. G. Larson, ''DNA molecular configurations in an evaporating droplet near a glass surface,'' J. Rheol. **47**, 1111–1132 (2003).

Coyle, D. J., ''Knife and roll coating,'' in *Liquid Film Coating. Scientific Principles and their Technological Implications*, edited by S. F. Kistler and P. M. Schweizer (Chapman and Hall, London, 1997), pp. 539–571.

Coyle, D. J., C. W. Macosko, and L. E. Scriven, ''Film-splitting flows in forward roll coating,'' J. Fluid Mech. **171**, 183–207 (1986).

Coyle, D. J., C. W. Macosko, and L. E. Scriven, ''Stability of symmetric film-splitting between counterrotating cylinders,'' J. Fluid Mech. **216**, 437–458 (1990).

Dontula, P., ''Polymer solutions in coating flows,'' Ph.D. thesis, University of Minnesota, Minneapolis, MN, 1999; available from UMI, Ann Arbor, MI, Order No. 9937847.

Flory, P. J., *Principles of Polymer Chemistry*, 1st ed. (Cornell University Press, Ithaca, NY, 1953).

Fuller, G. G., *Optical Rheometry of Complex Fluids* (Oxford University Press, New York, 1995).

Gaskell, P. H., G. E. Innes, and M. D. Savage, ''An experimental investigation of meniscus roll coating,'' J. Fluid Mech. **355**, 17–44 (1998).

Greener, Y., and S. Middleman, ''A theory of roll coating of viscous and viscoelastic fluids,'' Polym. Eng. Sci. **15**, 1–10 (1975).

Greener, J., T. Sullivan, B. Turner, and S. Middleman, ''Ribbing instability of a two-roll coater: Newtonian fluids,'' Chem. Eng. Commun. **5**, 73–10 (1980).

Haber, C., S. A. Ruiz, and D. Wirtz, ''Shape anisotropy of a single random-walk polymer,'' Proc. Natl. Acad. Sci. U.S.A. **97**, 10792–10795 (2000).

Hagerman, P. J., ''Flexibility of DNA,'' Annu. Rev. Biophys. Biophys. Chem. **17**, 265–286 (1988).
Harrison, G. M., J. Remmelgas, and L. G. Leal, ''The dynamics of ultradilute polymer solutions in transient flow: Comparison of dumbbell-based theory and experiment,'' J. Rheol. **42**, 1039–1058 (1998).
Haugland, R. P., *Handbook of Fluorescent Probes and Research Chemicals*, 6th ed. (Molecular Probes, Eugene, OR, 1996).
Hur, J. S., E. S. G. Shaqfeh, and R. G. Larson, ''Brownian dynamics simulations of single DNA molecules in shear flow,'' J. Rheol. **44**, 713–742 (2000).
Hur, J. S., E. S. G. Shaqfeh, H. P. Babcock, D. E. Smith, and S. Chu, ''Dynamics of dilute and semidilute DNA solutions in the start-up of shear flow,'' J. Rheol. **45**, 421–450 (2001).
Janeschitz-Kriegl, H., *Polymer Melt Rheology and Flow Birefringence* (Springer, Berlin, 1983).
Jendrejack, R. M., J. J. de Pablo, and M. D. Graham, ''Stochastic simulations of DNA in flow: Dynamics and the effects of hydrodynamic interaction,'' J. Chem. Phys. **116**, 7752–7759 (2002).
Jendrejack, R. M., D. C. Schwartz, J. J. de Pablo, and M. D. Graham, ''Shear-induced migration in flowing polymer solutions: Simulation of long-chain DNA dynamics in microchannels,'' J. Chem. Phys. **120**, 2513–2529 (2004).
Jendrejack, R. M., E. T. Dimalanta, D. C. Schwartz, M. D. Graham, and J. J. de Pablo, ''DNA dynamics in a microchannel,'' Phys. Rev. Lett. **91**, 038102 (2003).
Kam, Z., N. Borochov, and H. Eisenberg, ''Dependence of laser light scattering of DNA on NaCl concentration,'' Biopolymers **20**, 2671–2690 (1981).
Larson, R. G., H. Hu, D. E. Smith, and S. Chu, ''Brownian dynamics simulations of a DNA molecule in an extensional flow field,'' J. Rheol. **43**, 267–304 (1999).
Larson, R. G., T. T. Perkins, D. E. Smith, and S. Chu, ''Hydrodynamics of a DNA molecule in a flow field,'' Phys. Rev. E **55**, 1794–1797 (1997).
Le Duc, P., C. Haber, G. Bao, and D. Wirtz, ''Dynamics of individual flexible polymers in a shear flow,'' Nature (London) **399**, 564–566 (1999).
Morikawa, K., and M. Yanagida, ''Visualization of individual DNA molecules in solution by light microscopy: DAPI staining method,'' J. Biochem. (Tokyo) **89**, 693–696 (1981).
Papanastasiou, T. C., N. Malamantaris, and K. Ellwood, ''A new outflow boundary condition,'' Int. J. Numer. Methods Fluids **14**, 587–608 (1992).
Pasquali, M., ''Polymer molecules in free surface coating flows,'' Ph.D. thesis, University of Minnesota, Minneapolis, MN, 2000; available from UMI, Ann Arbor, MI, Order No. 9963019.
Pasquali, M., and L. E. Scriven, ''Free surface flows of polymer solutions with models based on the conformation tensor,'' J. Non-Newtonian Fluid Mech. **108**, 363–409 (2002).
Perkins, T. T., ''Exploring polymer dynamics with single DNA molecules,'' Ph.D. thesis, Stanford University, Palo Alto, CA, 1997; available from UMI, Ann Arbor, MI, Order No. 9810187.
Perkins, T. T., D. E. Smith, and S. Chu, ''Direct observation of tube-like motion of a single polymer chain,'' Science **264**, 819–822 (1994b).
Perkins, T. T., D. E. Smith, and S. Chu, ''Single polymer dynamics in an elongational flow,'' Science **276**, 2016–2021 (1997).
Perkins, T. T., D. E. Smith, and S. Chu, ''Single polymers in elongational flows: Dynamic, steady-state and population averaged properties,'' in *Flexible Polymer Chain Dynamics in Elongational Flow: Theory and Experiment*, edited by T. Q. Nguyen and H. H. Kausch (Springer, Berlin, 1999), pp. 283–334.
Perkins, T. T., S. R. Quake, D. E. Smith, and S. Chu, ''Relaxation of a single polymer molecule observed by optical microscopy,'' Science **264**, 822–826 (1994a).
Perkins, T. T., D. E. Smith, R. G. Larson, and S. Chu, ''Stretching of a single tethered polymer in a uniform flow,'' Science **268**, 83–87 (1995).
Pitts, E., and J. Greiller, ''The flow of thin liquid films between rollers,'' J. Fluid Mech. **11**, 33–50 (1961).
Savage, M. D., ''Cavitation in lubrication. Part 1. On boundary conditions and cavity–fluid interfaces,'' J. Fluid Mech. **80**, 743–755 (1977).
Savage, M. D., ''Mathematical model for the onset of ribbing,'' AIChE J. **30**, 999–1002 (1984).
Schunk, P. R., and L. E. Scriven, ''Constitutive equation for modeling mixed extension and shear in polymer solution processing,'' J. Rheol. **34**, 1085–1119 (1990).
Shrewsbury, P. J., ''Flow of complex biological macromolecules in microfluidic devices,'' Ph.D. thesis, University of California, San Fransisco, CA and University of California, Berkeley, CA, 2000; available from UMI, Ann Arbor, MI, Order No. 9996538.
Shrewsbury, P. J., D. Liepmann, and S. J. Muller, ''Concentration effects of a biopolymer in a microfluidic device,'' Biomed. Microdevices **4**, 17–26 (2002).
Shrewsbury, P. J., S. J. Muller, and D. Liepmann, ''Effect of flow on complex biological macromolecules in microfluidic devices,'' Biomed. Microdevices **3**, 225–238 (2001).
Smith, D. E., ''Polymer physics experiments with single DNA molecules,'' Ph.D. thesis, Stanford University, Palo Alto, CA, 1999; available from UMI, Ann Arbor, MI, Order No. 9943720.
Smith, D. E., and S. Chu, ''Response of flexible polymers to a sudden elongational flow,'' Science **281**, 1335–1340 (1998).

Smith, D. E., H. P. Babcock, and S. Chu, ''Single-polymer dynamics in steady shear flow,'' Science **283**, 1724–1727 (1999).

Torazzi, R., ''Visualizzazione di singole molecole polimeriche in coating flows,'' Master's thesis (tesi di laurea), Università degli Studi di Bologna, Bologna, Italy, 1998.

Wang, Y., A. Warshawsky, C. Wang, N. Kahana, C. Chevallard, and V. Steinberg, ''Fluorescent ultrahigh-molecular-weight polyacrylamide probes for dynamic flow systems: Synthesis, conformational behavior and imaging,'' Macromol. Chem. Phys. **203**, 1833–1843 (2002).

Wilson, S. D. R., ''The drag-out problem in film coating theory,'' J. Eng. Math. **16**, 209–221 (1982).

Woo, N. J., E. S. G. Shaqfeh, and B. Khomami, ''The effect of confinement on dynamics and rheology of dilute deoxyribose nucleic acid solutions. II. Effective rheology and single chain dynamics,'' J. Rheol. **48**, 299–318 (2004a).

Woo, N. J., E. S. G. Shaqfeh, and B. Khomami, ''Effect of confinement on dynamics and rheology of dilute DNA solutions. I. Entropic spring force under confinement and a numerical algorithm,'' J. Rheol. **48**, 281–298 (2004b).

Yanagida, M., I. Hiroaka, and Y. Katsura, ''Dynamic behavior of DNA molecules in solution studied by fluorescence microscopy,'' Cold Spring Harbor Symp. Quant. Biol. **47**, 177–187 (1983).